

“The Role of Non-Conventional Supports for Single-Atom Platinum-Based Catalysts in Fuel-Cell Technology: A Theoretical Surface Science Approach”

5th February 2013

Name of Principal Investigators (PI and Co-PIs): Aloysius Soon

- e-mail address : aloysius.soon@yonsei.ac.kr
- Institution : Yonsei University, South Korea
- Mailing Address : 50 Yonsei-Ro, Seodaemun-Gu, 120-749, Seoul
- Phone : +82-10-2923-5839
- Fax : +82-2-312-5375

Period of Performance: January/30/2012 – January/29/2013

Abstract: As a first step towards a microscopic understanding of single-Pt atom-dispersed catalysts on non-conventional TiN supports, we present density-functional theory (DFT) calculations to investigate the adsorption properties of Pt atoms on the pristine TiN(100) surface, as well as the dominant influence of surface defects on the thermodynamic stability of platinized TiN. Optimized atomic geometries, energetics, and analysis of the electronic structure of the Pt/TiN system are reported for various surface coverages of Pt. We find that atomic Pt does not bind preferably to the clean TiN surface, but under typical PEM fuel cell operating conditions, i.e. strongly oxidizing conditions, TiN surface vacancies play a crucial role in anchoring the Pt atom for its catalytic function. Whilst considering the energetic stability of the Pt/TiN structures under varying N conditions, embedding Pt at the surface N-vacancy site is found to be the most favorable under N-lean conditions. Thus, the system of embedding Pt at the surface N-vacancy site on TiN(100) surface could be a promising catalyst for PEM fuel cells.

Introduction: Proton exchange membrane fuel cells (PEMFCs) have found wide potential applications in stationary power sources and mobile automobiles, largely due to their low operating temperatures, low carbon-emissions, and light weight. Unfortunately, due to their high cost and low lifespan, wide-scale commercialization of PEMFCs has been greatly impeded and much effort has been made to lower its cost as well as to improve its durability over time. In an attempt to alleviate the high-cost associated with conventional PEMFC catalysts and to further maximize its catalytic activity and durability, we propose a promising route to design the next generation of Pt-based PEMFC nanocatalysts with single-Pt atom dispersions and to replace the easily degraded carbon support with the more durable non-conventional nitride-based support – TiN, in hope to improve the lifetime of these PEMFCs.

Experiment: We employ the projector augmented-wave (PAW) method for the electron-ion interactions and the generalized-gradient approximation (GGA) due to Perdew, Burke and Ernzerhof (PBE) for the exchange-correlation functional in density-functional theory (DFT), as implemented in the Vienna *ab initio* Simulations

Report Documentation Page				Form Approved OMB No. 0704-0188	
Public reporting burden for the collection of information is estimated to average 1 hour per response, including the time for reviewing instructions, searching existing data sources, gathering and maintaining the data needed, and completing and reviewing the collection of information. Send comments regarding this burden estimate or any other aspect of this collection of information, including suggestions for reducing this burden, to Washington Headquarters Services, Directorate for Information Operations and Reports, 1215 Jefferson Davis Highway, Suite 1204, Arlington VA 22202-4302. Respondents should be aware that notwithstanding any other provision of law, no person shall be subject to a penalty for failing to comply with a collection of information if it does not display a currently valid OMB control number.					
1. REPORT DATE 15 FEB 2013		2. REPORT TYPE Final		3. DATES COVERED 30-01-2012 to 29-01-2013	
4. TITLE AND SUBTITLE The Role of Non-Conventional Supports for Single-Atom Platinum-Based Catalysts in Fuel-Cell Technology: A Theoretical Surface Science Approach				5a. CONTRACT NUMBER FA23861214017	
				5b. GRANT NUMBER	
				5c. PROGRAM ELEMENT NUMBER	
6. AUTHOR(S) Sze Lok Soon				5d. PROJECT NUMBER	
				5e. TASK NUMBER	
				5f. WORK UNIT NUMBER	
7. PERFORMING ORGANIZATION NAME(S) AND ADDRESS(ES) Yonsei University,50 Yonsei-Ro, Seodaemun-Gu,Seoul 120-749,Korea,NA,NA				8. PERFORMING ORGANIZATION REPORT NUMBER N/A	
9. SPONSORING/MONITORING AGENCY NAME(S) AND ADDRESS(ES) AOARD, UNIT 45002, APO, AP, 96338-5002				10. SPONSOR/MONITOR'S ACRONYM(S) AOARD	
				11. SPONSOR/MONITOR'S REPORT NUMBER(S) AOARD-124017	
12. DISTRIBUTION/AVAILABILITY STATEMENT Approved for public release; distribution unlimited					
13. SUPPLEMENTARY NOTES					
14. ABSTRACT This is the final report of a first step towards a microscopic understanding of single-Pt atom-dispersed catalysts on non-conventional TiN supports. The researcher presents density-functional theory (DFT) calculations to investigate the adsorption properties of Pt atoms on pristine TiN(100) surfaces, as well as the dominant influence of surface defects on the thermodynamic stability of platinumized TiN.					
15. SUBJECT TERMS fuel cells , Theoretical modeling, electrodes					
16. SECURITY CLASSIFICATION OF:			17. LIMITATION OF ABSTRACT Same as Report (SAR)	18. NUMBER OF PAGES 17	19a. NAME OF RESPONSIBLE PERSON
a. REPORT unclassified	b. ABSTRACT unclassified	c. THIS PAGE unclassified			

Package (VASP). With its PAW potentials, VASP combines the accuracy of all-electron methods with the computational efficiency of plane-wave approaches.

Using this computational setup, we 1) study the bulk properties of TiN; 2) determine the structure of pristine TiN surfaces under specific fuel cell operating conditions; and 3) calculate the binding energy of atomic Pt at all possible on-surface as well as surface vacancy adsorption sites as a function of its coverage.

We report optimized atomic geometries, energetics, and analysis of the electronic structure of the Pt/TiN system for various surface coverages of Pt.

Details can be found in the following published papers:

1. T.-H. Lee, B. Delley, C. Stampfl, and A. Soon, Environment-dependent nanomorphology of TiN: Influence of surface vacancies, *Nanoscale* **4**, 5183 (2012)
2. R. Q. Zhang, T.-H. Lee, B.-D. Yu, C. Stampfl, and A. Soon, The role of titanium nitride supports for single-atom platinum-based catalysts in fuel cell technology, *Phys. Chem. Chem. Phys.* **14**, 16552 (2012), in the Special issue on Computational Catalysis and Materials for Energy Production, Storage and Utilization

Results and Discussion: In summary, utilizing first-principles DFT calculations, TiN supports for single-atom platinum-based catalysts are investigated. It is found that Pt atom prefers to be embedded in the surface of TiN at the N vacancy sites. According to the binding energy of Pt atoms, with respect to that of bulk Pt, single Pt atoms could be stable on the N atomic vacancy site rather than forming Pt metal clusters. The substitutional adsorption of Pt atoms at Ti vacancy sites in bulk TiN is energetically unfavorable. We found that atomic Pt does not bind preferably to the clean TiN surface, but under typical PEM fuel cells operational conditions, i.e. strongly oxidizing conditions, TiN surface vacancies play a crucial role in anchoring the Pt atom for its catalytic function. Whilst considering the energetic stability of the Pt/TiN structures under varying N conditions, embedding Pt at the surface N-vacancy site is found to be the most favorable under N-lean conditions, where Pt presents negative charge.

In order to realize the application of this platinized TiN surface in PEMFCs, further research is being pursued to 1) study the various adsorption of molecular fragments on the Pt/TiN electrode, as well as to 2) investigate the stability of Pt/TiN electrodes in different electrolytes via surface Pourbaix diagrams.

List of Publications and Significant Collaborations that resulted from your AOARD supported project:

Published papers in peer-reviewed journals

3. T.-H. Lee, B. Delley, C. Stampfl, and A. Soon, Environment-dependent nanomorphology of TiN: Influence of surface vacancies, *Nanoscale* **4**, 5183 (2012)
4. R. Q. Zhang, T.-H. Lee, B.-D. Yu, C. Stampfl, and A. Soon, The role of

titanium nitride supports for single-atom platinum-based catalysts in fuel cell technology, *Phys. Chem. Chem. Phys.* **14**, 16552 (2012), in the Special issue on Computational Catalysis and Materials for Energy Production, Storage and Utilization

Conference presentations without papers

1. Oral presentation at the American Physical Society (APS) March Meeting, Boston, MA, USA (2012)
2. Oral presentation at the 244th American Chemical Society (ACS) Fall Meeting, Philadelphia, USA (2012)

Cite this: *Nanoscale*, 2012, **4**, 5183www.rsc.org/nanoscale

PAPER

Environment-dependent nanomorphology of TiN: the influence of surface vacancies

Taehun Lee,^a Bernard Delley,^b Catherine Stampff^c and Aloysius Soon^{*a}

Received 23rd May 2012, Accepted 20th June 2012

DOI: 10.1039/c2nr31266b

In this work, we present density-functional theory calculations to investigate the surface properties of TiN as a function of surface orientation and termination, as well as the influence of surface defects for various surface defect concentrations. We calculate both the surface energies (including vacancy formation) as a function of the nitrogen chemical potential, and plot the first-principles derived equilibrium crystal shape (ECS) under different growth conditions. We find that surface defects can considerably change the derived ECS of TiN (especially under nitrogen-lean conditions), highlighting the importance of surface defect consideration in modeling nanoparticle morphology.

Introduction

Titanium nitride (TiN) is one of the classical refractory transition-metal nitrides and it crystallizes in the rocksalt (B1) structure. The close-packed B1 structure hinders the migration of species, with the result of excellent thermal and chemical stability against, for example, oxidation or self-diffusion.^{1–3} Because of its exceptional thermal and mechanical properties such as high melting point, high hardness, good thermal conductivity and high resistance to corrosion, TiN films have been used in various industrial applications such as hard wear-resistant coatings on cutting tools and corrosion-resistant coatings on mechanical components.⁴ More recently, titanium nitride nanoparticles have been demonstrated to be a robust support material for the Pt catalyst used in the proton exchange membrane fuel cells (PEM FCs).^{5–7} Electrodeposited Pt on TiN (or platinized TiN) often shows much higher catalytic performance than conventional Pt/C electrocatalysts as well as mitigating the CO poisoning effect (which is attributed to the presence of TiN).^{8,9}

With regards to its performance in these technological applications, it has been found to be strongly dependent on both its surface morphology and orientation of nanocrystallite grains.^{10–13} Although the exceptional thermal and mechanical properties of TiN are highly dependent on the film's microstructure, the underlying mechanisms and pathways leading to the development of preferred orientation in polycrystalline TiN layers are still poorly understood. The importance of having a good understanding of its preferred orientation is easily motivated by the fact that the morphology of isolated nanoparticles is dependent on the characteristics of exposed surface facets.¹⁴

Moreover, several studies have also probed the electronic and mechanical properties of bulk TiN as a function of its point defects.^{15–18} Nitrogen vacancies, V_N , in particular, are regarded as the primary defects that control the composition ratio of sub-stoichiometric TiN.^{19–21} However, the effect of sub-stoichiometry on the morphology of TiN still remains an open question. Furthermore, others have attempted to study the surface energetics and predict the shape of TiN nanoparticles *via* thermodynamics considerations,^{22–25} however no explicit account of bulk or surface defects were included in these studies.

Due to the high surface-to-volume ratios in TiN nanostructures, even small variations in the surface adsorption and defect behaviours, as well as the electronic properties of particular surface facets present on the nanoparticles, can have a huge effect on the overall performance of this nanomaterial.

In this present work, we perform first-principles density-functional theory (DFT) calculations to study the surface energetics of TiN as a function of surface orientation and termination. Surface defects (*i.e.* mono- and di-vacancies of Ti and N) for various surface defect concentrations are also investigated and the surface energies of these defect surfaces are compared and contrasted with those of the clean, defect-free surfaces. Extending our DFT calculations by using *ab initio* atomistic thermodynamics and the Gibbs–Wulff theorem,^{26,27} we then study the dependence of these surface energies as a function of the nitrogen chemical potential, and plot the first-principles derived nanomorphology under different growth conditions.

Methodology

All DFT calculations are performed using the all-electron DMol³ code,^{28,29} where we employ the generalized gradient approximation (GGA) of Perdew *et al.*³⁰ for the exchange-correlation functional. This code employs fast converging three-dimensional numerical integrations to calculate the matrix elements occurring

^aDepartment of Materials Science and Engineering, Yonsei University, Seoul 120-749, Korea. E-mail: aloyusius.soon@yonsei.ac.kr

^bPaul-Scherrer-Institut, CH-5232 Villigen PSI, Switzerland

^cSchool of Physics, The University of Sydney, Sydney, New South Wales 2006, Australia

in the Ritz variational method. The wave functions are expanded in terms of a double-numerical quality localized basis set with a real-space cutoff of 7.32 Bohr for nitrogen and 11.10 Bohr for titanium. More details can be found elsewhere.^{28,29,31}

To represent the clean and various TiN surfaces with defects, we use supercells containing symmetric slabs (with inversion symmetry) with 3 to 13 atomic layers and a vacuum region of 25 Å between adjacent slabs. All surfaces are fully relaxed while keeping the inner-most three center layers fixed at bulk values. The Brillouin-zone (BZ) is sampled by adopting the Monkhorst–Pack *k*-point grids of (12 × 12 × 1), (6 × 6 × 1) for the *p*(1 × 1) and *p*(2 × 2) TiN low-index surfaces, respectively. For all orientations we have verified that using thicker slabs does not result in any significant change (*i.e.* ≤ 1 meV Å⁻² for surface energies). We use the *p*(1 × 1) surface unit cell to study the low-index defect-free surfaces of TiN and a *p*(2 × 2) surface supercell to investigate surfaces containing defects.

Ab initio atomistic thermodynamics

In order to describe the thermodynamic stability of TiN surfaces in its immediate environment, we used the results of DFT total-energy calculations as an input to the atomistic thermodynamics model.^{32–34} In this approach, the most stable surface structure minimizes the surface Gibbs free energy, which is defined as,

$$\gamma(\mu_i) = \frac{1}{A} \left[G^{\text{surf}} - \sum_i N_i \mu_i(p_i, T) \right] \quad (1)$$

here, G^{surf} is the Gibbs free energy of the solid surface with the surface area A . μ_i is the chemical potential of the various species i present in the system, where in this study $i = \text{Ti}$ and N . N_i is the number of atoms of the species i . For a given sufficiently large nanoparticle of TiN, bulk TiN may be assumed to be the thermodynamic reservoir with which the surface is equilibrated. This then constrains the chemical potentials of Ti (μ_{Ti}) and N (μ_{N}) to the Gibbs free energy (per formula unit) of bulk TiN, $g_{\text{TiN}}^{\text{bulk}}$, *i.e.*

$$g_{\text{TiN}}^{\text{bulk}} = \mu_{\text{Ti}} + \mu_{\text{N}}. \quad (2)$$

Given that eqn (2) holds true, we can now re-formulate eqn (1), expressing the surface free energy solely as a function of μ_{N} .

$$\gamma(\mu_{\text{N}}) = \frac{1}{A} \left[G^{\text{surf}} - N_{\text{Ti}} g_{\text{TiN}}^{\text{bulk}} - (N_{\text{N}} - N_{\text{Ti}}) \mu_{\text{N}} \right]. \quad (3)$$

This formulation will allow one to include the energy cost of defect formation when calculating the surface energies of the TiN surfaces with defects, as well as for the polar N- and Ti-terminated TiN(111) surfaces that deviate from bulk stoichiometry. From previous studies,^{26,35} the vibrational contributions to the Gibbs free energy of solid surfaces are found to be typically small, and are thus neglected in this work. Hence, G^{surf} is approximated by the total energies as obtained from our DFT calculations. For more details, we refer to ref. 31 and references therein. We note that it is often convenient to express the dependence of the surface energy on $\Delta\mu_{\text{N}}$, where $\Delta\mu_{\text{N}} = \mu_{\text{N}} - \frac{1}{2}E_{\text{N}_2}$, which simply translates the chemical potential scale by half the total energy of the nitrogen molecule (*i.e.* $\frac{1}{2}E_{\text{N}_2}$). To further relate this chemical potential change to more intuitive pressure–temperature (p , T) relations,^{32,33} based on the ideal-gas

laws, we will convert the dependence of the surface free energy on (p , T) into pressure scales at $T = 800$ and 2000 K.

Gibbs–Wulff theory of the equilibrium crystal shape

Having obtained accurate first-principles surface Gibbs free energies, $\gamma(\mu_{\text{N}})$, we can then utilize these surface energies as *ab initio* input parameters into a simple model to predict the morphology of TiN nanoparticles – the Gibbs–Wulff theory of equilibrium crystal shape (ECS).^{22,26,27,36–38} As we are only using the surface energies of low-index TiN surfaces, we are essentially predicting a constrained ECS, confined by these low-index surfaces. In fact, it has been shown from experiments that the as-synthesized crystals are typically terminated by low-index surfaces, thus higher-index surfaces may not have a strong influence on the nanoparticle shape.

The Gibbs–Wulff theory provides a simple mathematical approach that predicts the ECS of crystals or nanoparticles, whereby the total free energy of the crystal is minimum at a constant volume. The predicted ECS is then termed as a Wulff construction. The mathematical expression for this energy–shape relation is as follows:

$$r(\mathbf{d}) = \min_{hkl} [\alpha \cdot \gamma(\mu_i)], \quad (4)$$

where $r(\mathbf{d})$ represents the radius of the crystal shape in the direction of the vector, \mathbf{d} and α is the proportionality constant. The directional vector, \mathbf{d} , defines the normal vector to a particular crystal surface (hkl). At a distance from the origin numerically equal to the surface free energy, $\gamma(\mu_{\text{N}})$ of that surface, a normal plane is established. Consequently, one returns to the origin and reiterates this process for all other crystallographic directions. In this way, the smallest volume enveloping the origin inside all these planes can then be taken, in a geometrical sense, as the minimum-energy morphology for a particular nanocrystal. In this work, since the surface free energy of TiN can also be expressed as a function of the chemical potential of interest (μ_{N}), this further allows a rather straightforward extension of the Wulff construction to include its dependence on μ_{N} .

Results and discussion

Bulk TiN

TiN crystallizes in a rock-salt B1 structure with the space group $Fm\bar{3}m$. There are two formula units of TiN in this conventional unit cell of 8 atoms: Ti atoms at (0,0,0), ($\frac{1}{2}, \frac{1}{2}, 0$), ($\frac{1}{2}, 0, \frac{1}{2}$), (0, $\frac{1}{2}, \frac{1}{2}$) and N atoms at (0,0, $\frac{1}{2}$), (0, $\frac{1}{2}, 0$), ($\frac{1}{2}, 0, 0$), ($\frac{1}{2}, \frac{1}{2}, \frac{1}{2}$), as shown Fig. 1a. The total density-of-states is presented in Fig. 1b, clearly showing that TiN is a metal with occupied states at the Fermi level.

The equilibrium lattice constant, a_0 , of TiN is calculated to be 4.25 Å which is close to the experimental value of 4.24 Å and agrees well with the other reported DFT-GGA values, ranging from 4.23 to 4.26 Å.^{23–25,31,39} The computed bulk modulus is 275.5 GPa, which compares well with the corresponding experimental value of 288 GPa⁴⁰ and the theoretical value of 280 GPa.³¹ For the N₂ molecule, the binding energy per N atom is calculated to be −5.17 eV, which agrees well with the reported theoretical value of −5.19, ref. 41, which is typically overbound when

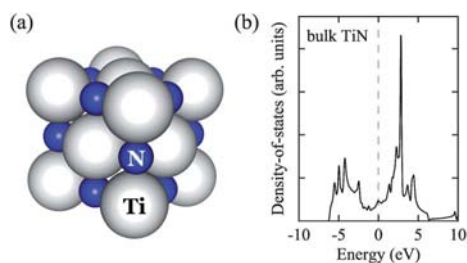


Fig. 1 (a) Crystal structure of bulk titanium nitride, TiN. The titanium and nitrogen atoms are shown as large white and small grey (blue) spheres, respectively. (b) Total density-of-states of bulk TiN, with the Fermi energy indicated by the vertical dashed line at 0 eV.

compared to the reported experimental value of -4.97 eV.²⁴ The enthalpy of formation of TiN (with respect to the bulk Ti metal and N_2 gas) is found to be -3.39 eV per formula unit which is in good agreement with the reported theoretical value of -3.56 eV.³⁹

Low-index TiN surfaces: without surface defects

In this work, we consider the three low-index surfaces of TiN, namely the (100), (110) and (111) surfaces. We note that the (111) surface bears two different surface terminations – the N-terminated [*i.e.* TiN(111):N] and the Ti-terminated [*i.e.* TiN(111):Ti] surface. The top- and side-views of the atomic geometries of these surfaces are shown in Fig. 2 accordingly. For TiN(100), surface relaxation effects are moderate, with interlayer relaxations of less than 1% when compared to bulk truncated spacings. On the other hand, TiN(111):N and TiN(111):Ti experience much larger relaxations – as much as a contraction of 37% for the outermost layer for TiN(111):N and a contraction of 11% for that of TiN(111):Ti. The corresponding surface relaxation of TiN(110) is a little milder, *i.e.* an outermost layer contraction of less than 10%. These findings are very much in line with those found in ref. 25.

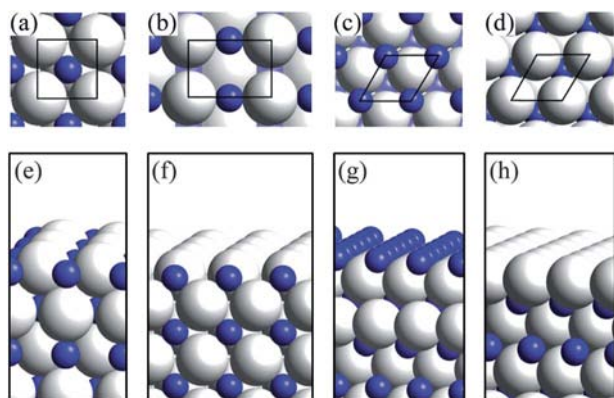


Fig. 2 Surface structures of TiN. (a) to (d) show the top-view of TiN(100), TiN(110), TiN(111):N, and TiN(111):Ti, respectively. The N- and Ti-terminated (111) surfaces of TiN are labelled as TiN(111):N and TiN(111):Ti accordingly. Their corresponding side-views are shown in (e) to (h). The titanium atoms are shown as large white spheres, and the nitrogen atoms as small grey (blue) spheres.

Using eqn (3), we calculate the surface energies of these low-index surfaces under both N-rich and N-lean conditions, and report them in Table 1 and the values are plotted in Fig. 3a. Given that both the (100) and (110) surfaces of TiN are stoichiometric with respect to bulk stoichiometry, their calculated surface energies are independent of the nitrogen chemical potential variation. However, for both non-stoichiometric TiN(111):N and TiN(111):Ti, their surface energies then vary linearly as a function of $\Delta\mu_N$, with the N-rich TiN(111):N surface more stable under N-rich conditions, and the Ti-rich TiN(111):Ti surface more stable under N-lean conditions.

Now that we have determined the relative surface energies of these (defect-free) low-index surfaces of TiN as a function of $\Delta\mu_N$, we can use the Gibbs–Wulff theorem (*cf.* eqn (4)) to determine the environment-dependent nanomorphology of TiN. The ECS for both N-lean and N-rich conditions are plotted in Fig. 3b and c, respectively. Given that the $\gamma(\Delta\mu_N)$ in Fig. 3a is symmetric about the center of the $\gamma(\Delta\mu_N)$ plot, the resulting ECSs are virtually identical at both extreme growth conditions. The morphology of TiN is that of a truncated cube, *i.e.* with the eight vertices at the corners of the cube cropped off. Based on the ECS, we see that the dominant facet is {100}, followed by that of {111}.

As in most reported results,^{22–25} this would be commonly taken as the conclusive morphology if one considers only bulk-truncated, defect-free surfaces. In the following, we will show that this premature conclusion can be a little misleading, as in the case of nanoparticles of TiN.

Low-index TiN surfaces: with surface defects

Experimentally, TiN is known to be nitrogen-deficient (*i.e.* contains N vacancies, V_N).^{19–21} Thus, to include the influence of surface vacancies in our investigation, we calculate and study the stability of surface mono- and di-vacancies of N and Ti on the low-index surfaces of TiN. To do this, we consider V_N and V_{Ti} in a $p(2 \times 2)$ surface cell. The top-view of the atomic geometry of the mono-vacancy of N and Ti on TiN(100) is shown in Fig. 4a and d, respectively. The di-vacancies of N on this surface are shown in Fig. 4b and c [labelled as “(100) $2V_N$ -trans” and “(100) $2V_N$ -adj”], while those of Ti are shown in Fig. 4e and f [labelled as “(100) $2V_{Ti}$ -trans” and “(100) $2V_{Ti}$ -adj”], respectively, as there are two ways of creating the di-vacancies (*i.e.* the “trans” and “adj” way) on this surface. The mono- and di-vacancies of N on the TiN(111):N surface are shown in Fig. 4g and h, while that of Ti on TiN(111):Ti in Fig. 4i and j, accordingly. Fig. 4k and o depict the mono-vacancy of N and Ti on TiN(110), respectively. The di-vacancies of N are shown in Fig. 4l–n [denoted as “(110)

Table 1 Surface free energies (in eV \AA^{-2}) of the three low-index surfaces of TiN, namely TiN(100), TiN(110), and TiN(111) with N- and Ti-surface terminations [TiN(111):N and TiN(111):Ti, respectively], under both N-lean and N-rich conditions

Surfaces	$\gamma_{N\text{-lean}}$	$\gamma_{N\text{-rich}}$
(100)	0.077	0.077
(110)	0.167	0.167
(111):N	0.323	0.107
(111):Ti	0.109	0.325

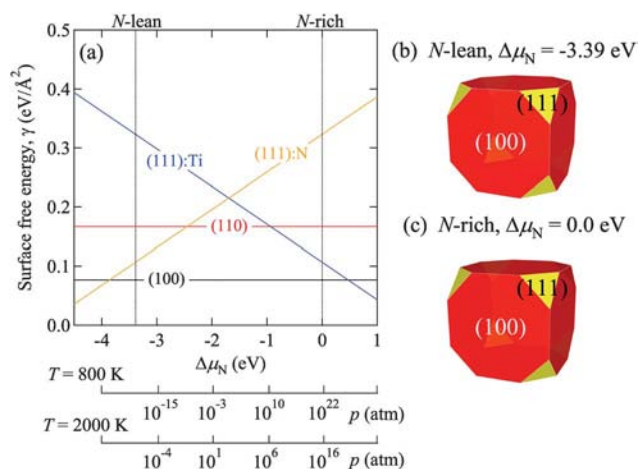


Fig. 3 (a) Calculated surface free energy (as a function of the change in the chemical potential of nitrogen, $\Delta\mu_{\text{N}}$) of the three low-index surfaces of TiN, namely TiN(100), TiN(110), and TiN(111) with N- and Ti-surface terminations [TiN(111):N and TiN(111):Ti, respectively]. The corresponding pressure bar lines at $T = 800$ and 2000 K are shown. Under both N-lean and N-rich conditions, the equilibrium crystal shapes (as determined by the Gibbs–Wulff theorem) are also shown in both (b) and (c) accordingly, and are found to be identical. No surface defects are considered in this plot.

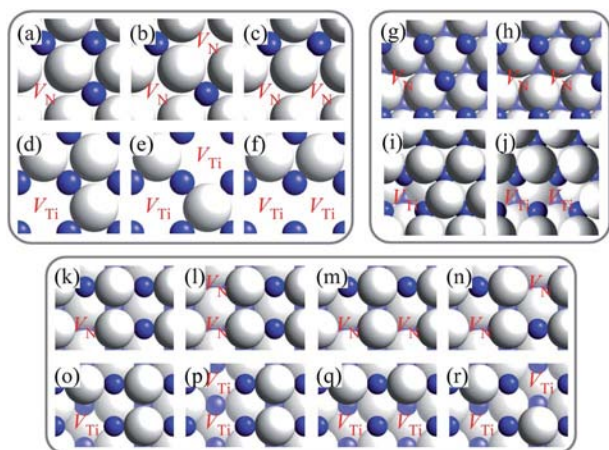


Fig. 4 Top-view of the atomic structures of TiN with various surface vacancies. (a) and (d) show the mono-vacancy of N and Ti on TiN(100), respectively. The di-vacancies of N are shown in (b) and (c) [denoted as “(100) $2V_{\text{N-trans}}$ ” and “(100) $2V_{\text{N-adj}}$ ”], while those of Ti are shown in (e) and (f) [denoted as “(100) $2V_{\text{Ti-trans}}$ ” and “(100) $2V_{\text{Ti-adj}}$ ”], respectively. The mono- and di-vacancies of N on the TiN(111):N surface are depicted in (g) and (h), while that of Ti on TiN(111):Ti in (i) and (j), accordingly. (k) and (o) show the mono-vacancy of N and Ti on TiN(110), respectively. The di-vacancies of N are shown in (l), (m) and (n) [denoted as “(110) $2V_{\text{N-adj}}$ ”, “(110) $2V_{\text{N-opps}}$ ” and “(110) $2V_{\text{N-trans}}$ ”], while those of Ti are shown in (p), (q) and (r) [denoted as “(110) $2V_{\text{Ti-adj}}$ ”, “(110) $2V_{\text{Ti-opps}}$ ” and “(110) $2V_{\text{Ti-trans}}$ ”], respectively. Here, the titanium atoms are shown as large white spheres and the nitrogen atoms as small grey (blue) spheres while the vacancy site is labelled as V_{N} and V_{Ti} for the N vacancy and Ti vacancy, respectively.

$2V_{\text{N-adj}}$, “(110) $2V_{\text{N-opps}}$ ” and “(110) $2V_{\text{N-trans}}$ ”, while those of Ti are shown in Fig. 4p–r [denoted as “(110) $2V_{\text{Ti-adj}}$ ”, “(110) $2V_{\text{Ti-opps}}$ ” and “(110) $2V_{\text{Ti-trans}}$ ”], accordingly. As in this case

of TiN(110), there exist three ways to create di-vacancies (*i.e.* the “trans”, “opps”, and “adj” way) on this surface.

In a similar fashion, we calculate the surface energies of these defect surfaces, using eqn (3), and report their values for both the N-rich and N-lean conditions in Table 2, and plot their dependence on $\Delta\mu_{\text{N}}$ in Fig. 5a. Interestingly, we find that a few structures containing surface defects (*e.g.* (100) $2V_{\text{N-adj}}$ and (100) V_{N}) are found to compete in stability with those that are defect-free. We also find that the mono-vacancies are generally favoured over the di-vacancies, suggesting that a repulsive lateral interaction exists between these surface defects and thus they do not prefer to be in close proximity to one another. More importantly, the relative stability amongst these low-index surfaces is greatly modified by the presence of these surface vacancies. Now, we feed our first-principles derived surface energies (now including surfaces with defects) into the Gibbs–Wulff equation (eqn (4)) and we find that the previous predicted ECSs does not hold true anymore. The new ECSs that include a more realistic treatment of surface defects are shown in Fig. 5b for the N-lean condition, and in Fig. 5c for the N-rich condition.

Here we find that the new ECSs are asymmetric when compared to that where surface vacancies were not considered (see Fig. 3b and c); under N-lean conditions, the dominance of the (100)-type is clearly seen, yielding a cubic morphology enclosed by the {100} facets, unlike the case when surface defects were not considered. It is clear that other surface structures in the {110} and {111} direction are much less stable as compared to the thermodynamically stable (100) V_{N} structure. As the chemical potential of N increases, *i.e.* moving towards the right of the plot in Fig. 5a, we find that the defect-free, stoichiometric TiN(100) surface becomes the most stable after $\Delta\mu_{\text{N}} = -2.9$ eV. However, again reminding that one should consider the relative stability of surface energies rather than simply the absolute numbers, we see that the morphology of TiN under N-rich

Table 2 Surface free energies (in $\text{eV } \text{\AA}^{-2}$) of various considered TiN surfaces (including surfaces with mono- and di-vacancies of N and Ti) under both N-lean and N-rich conditions

Surfaces		$\gamma_{\text{N-lean}}$	$\gamma_{\text{N-rich}}$
(100)	defect-free	0.077	0.077
	V_{N}	0.062	0.155
	$2V_{\text{N-adj}}$	0.071	0.258
	$2V_{\text{N-trans}}$	0.079	0.265
	V_{Ti}	0.184	0.091
	$2V_{\text{Ti-adj}}$	0.317	0.131
	$2V_{\text{Ti-trans}}$	0.354	0.167
(110)	defect-free	0.167	0.167
	V_{N}	0.147	0.214
	$2V_{\text{N-adj}}$	0.123	0.256
	$2V_{\text{N-opps}}$	0.148	0.280
	$2V_{\text{N-trans}}$	0.124	0.256
	V_{Ti}	0.203	0.137
	$2V_{\text{Ti-adj}}$	0.258	0.126
(111):N	defect-free	0.323	0.107
	V_{N}	0.242	0.134
	$2V_{\text{N-trans}}$	0.182	0.182
	defect-free	0.107	0.323
	$2V_{\text{Ti}}$	0.152	0.260
	$2V_{\text{Ti-trans}}$	0.191	0.191

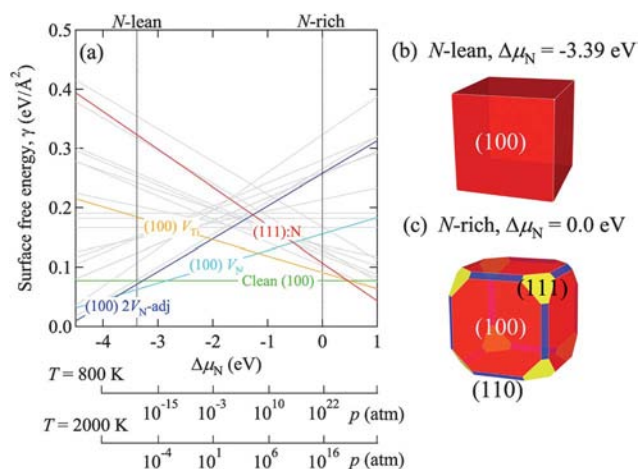


Fig. 5 (a) Calculated surface free energy (as a function of the change in the chemical potential of nitrogen, $\Delta\mu_N$) of various considered surfaces of TiN (including surfaces with mono- and di-vacancies of N and Ti), with the corresponding pressure bar lines at $T = 800$ and 2000 K. Under N-lean conditions, the TiN(100) surface with two adjacent nitrogen vacancies [(100) $2V_{N\text{-adj}}$, Fig. 4c] is found to be stable, while the defect-free TiN(100) surface is stable for more higher chemical potentials of N. Under both N-lean and N-rich conditions, the equilibrium crystal shapes (as determined by the Gibbs–Wulff theorem) are shown in both (b) and (c) accordingly, and are found to be different from that in Fig. 3. Other unfavourable phases are indicated by pale gray lines.

conditions now reveals an additional facet – {110}, which was not shown in the ECS obtained using only defect-free surface energies, in addition to the {111} facet once again appearing, truncating the {100} cube.

Experimentally, the morphology of nanocrystallites of TiN was first studied by Bentzon and Kragh using high-resolution transmission electron microscopy (HR-TEM).⁴² They evaporated Ti at about 2000 K in an atmosphere of He and N_2 , at a N_2 partial pressure of about 100 to 300 Pa ($\sim 10^{-3}$ atm), to synthesize very small nanoparticles of TiN, ranging from 5 to 20 nm in size. To estimate the nitrogen content of these nanoparticles, the authors used the electron energy loss spectroscopy technique and found the atomic weight percentage of N to be close to 33% – arguably resembling the N-deficient structures that are stabilized under N-lean conditions, corresponding to a nitrogen partial

pressure of $\sim 10^{-4}$ atm at 2000 K (see Fig. 5a). It is gratifying to find that the explicit shapes seen for most of the TiN nanocrystallites under these matching growth conditions are predominantly cubic. It is clear that if surface defects of TiN were ignored in the thermodynamic shape model, the predicted morphology of the TiN nanocrystallites may not agree well with that of the observed HR-TEM images, highlighting the importance of considering surface defects for a more realistic approach towards morphological modelling.

Electronic structure

Now, turning to the electronic structure of these low-energy surfaces, namely the TiN(100) V_N and the defect-free TiN(100) surfaces under N-lean and N-rich conditions respectively, we calculate their electronic density-of-states (DOS) in Fig. 6. In Fig. 6a, we see that the general shape of the total DOS is not greatly changed when comparing the bulk material and its (100) surfaces, with the exception of the states from -5 to 0 eV. To scrutinize this change in the DOS, we plot and study the partial DOS for the Ti 3d, and the N 2p states in Fig. 6b and c, respectively. For the Ti 3d states, we see that the states in the energy range of -5 to -3 eV move up in energy (*i.e.* closer to the Fermi level) when comparing that of the bulk TiN to that of the defect-free TiN(100) surface. With regards to the (100) surface with a surface nitrogen vacancy, TiN(100) V_N , the same behaviour is observed. In addition, we find that near the Fermi level, a new surface defect state at -1.5 eV appears, upon the creation of V_N (see Fig. 6b, indicated by a downward-pointing arrow). This suggests that upon generating a surface N vacancy, the 3d states of the neighbouring Ti atoms re-align to accommodate the extra transferred charges, resulting in an occupied surface defect-induced Ti 3d state near the Fermi-level. Turning now to the N 2p states (in Fig. 6c), again we notice that these states are generally up-shifted closer to the Fermi level. Here, we can see a more dramatic narrowing of the N 2p states upon creating the (100) surface as opposed to that of bulk TiN. As seen from the partial DOS, the N 2p state of the nearest neighbouring surface N in the TiN(100) V_N structure narrows even further upon creating the V_N .

To provide some “quantitative” description of these charge re-distributions, we also calculate the Mulliken atomic charges for bulk TiN, TiN(100), and TiN(100) V_N . Given that the

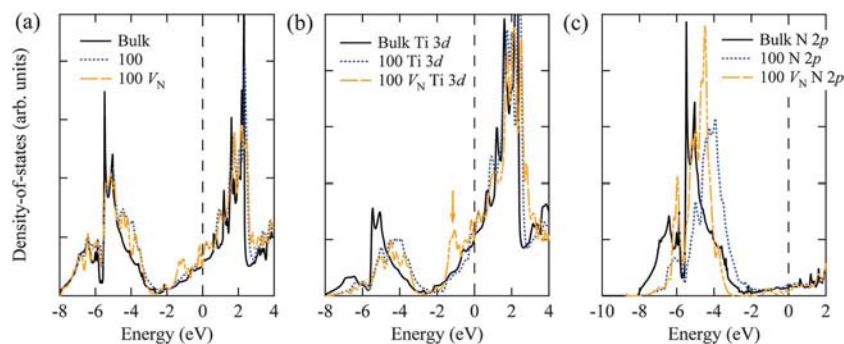


Fig. 6 (a) Total density-of-states (DOS) of bulk TiN (solid line), TiN(100) (dotted line), and TiN V_N (dot-dashed line). The corresponding partial DOS for Ti and N are plotted and labelled in (b) and (c), respectively. In (b), the position of the new surface defect Ti 3d state is marked by a downward-pointing arrow. For all plots, the Fermi energy is indicated by the vertical dashed line at 0 eV.

accuracy of these charge partitioning techniques is highly sensitive to the quality of the basis sets used in the calculation, we focus here on the *relative change* in the atomic charges with respect to bulk TiN (Δq), rather than their absolute values. Thus, we find that upon creating the defect-free TiN(100) surface, Δq for the outermost Ti and N surface atoms are -0.01 and $0.07 |e|$, which is quite small, especially for the surface Ti atom. However upon creating a V_N on the (100) surface, Δq for the neighbouring surface Ti and N atoms are found to be -0.20 and $0.09 |e|$, respectively, showing a significant increase in Δq for the surface Ti atom nearest to the V_N . This charge analysis reaffirms the changes we see in the partial DOS mentioned above.

Conclusions

In summary, we perform DFT calculations for the (100), (110), and (111) low-index surfaces of TiN. In particular, we calculate the surface energy for the defect-free and surface vacancy containing surfaces and present these energies as a function of the nitrogen chemical potential. Importantly, we find that N surface vacancies on TiN(100) are stable under N-lean growth conditions, and only when these surface defects are taken into account and included in our first-principles DFT-based Gibbs–Wulff model do we find good agreement with the cubic shapes determined by HR-TEM, especially under N-lean growth conditions. Given that defects occur naturally in many technologically important nanomaterials, *e.g.* metal oxides and nitrides, and where the overall shape of the nanoparticle could greatly influence its overall material performance (*e.g.* in nanocatalysts), we propose that surface defects will play a considerable role and should be taken into account in nanomorphological predictions.

Acknowledgements

The authors gratefully acknowledge support from the Korean Ministry of Education, Science, and Technology (MEST) through an institutional research program of the Korea Institute of Science and Technology (KIST) (Contract no. 2E22731), the Australian Research Council (ARC) and partially funded by the Asian Office of Aerospace Research and Development (AOARD, Award No. FA2386-12-1-4017). Computational resources have been provided by the Korea Institute of Science and Technology Information (KISTI) supercomputing center through the strategic support program for the supercomputing application research (KSC-2011-C2-39), as well as the Australian National Computational Infrastructure (NCI).

References

- 1 S. Jhi, J. Ihm, S. Louie and M. Cohen, *Nature*, 1999, **399**, 132.
- 2 L. Hultman, *Vacuum*, 2000, **57**, 1.
- 3 F. Lévy, P. Hones, P. E. Schmid, R. Sanjinés, M. Diserens and C. Wiemer, *Surf. Coat. Technol.*, 1999, **120–121**, 284.
- 4 P. H. Mayrhofer, C. Mitterer, L. Hultman and H. Clemens, *Prog. Mater. Sci.*, 2006, **51**, 1032.
- 5 B. Avasara, T. Murray, W. Li and P. Haldar, *J. Mater. Chem.*, 2009, **19**, 1803.
- 6 B. Avasara and P. Haldar, *Int. J. Hydrogen Energy*, 2011, **36**, 3965.
- 7 R. Q. Zhang, T. H. Lee, B. D. Yu, C. Stampfl and A. Soon, *Phys. Chem. Chem. Phys.*, 2012, DOI: 10.1039/C2CP41392B.
- 8 O. T. M. Musthafa and S. Sampath, *Chem. Commun.*, 2008, 67.
- 9 M. M. Ottakam Thotiyl, T. Ravikumar and S. Sampath, *J. Mater. Chem.*, 2010, **20**, 10643.
- 10 U. C. Oh and J. H. Je, *J. Appl. Phys.*, 1993, **74**, 1692.
- 11 J. E. Greene, J.-E. Sundgren, L. Hultman, I. Petrov and D. B. Bergstrom, *Appl. Phys. Lett.*, 1995, **67**, 2928.
- 12 J. H. Je, D. Y. Noh, H. K. Kim and K. S. Liang, *J. Appl. Phys.*, 1997, **81**, 6126.
- 13 K. Min, S. Hofmann and R. Shimizu, *Thin Solid Films*, 1997, **295**, 1.
- 14 M. J. Yacamán, J. A. Ascencio, H. B. Liu and J. Gardea-Torresdey, *J. Vac. Sci. Technol., B: Microelectron. Nanometer Struct.–Process. Meas., Phenom.*, 2001, **19**, 1091.
- 15 L. Tsetseris, N. Kalfagiannis, S. Logothetidis and S. T. Pantelides, *Phys. Rev. B: Condens. Matter Mater. Phys.*, 2007, **76**, 224107.
- 16 L. Tsetseris, N. Kalfagiannis, S. Logothetidis and S. T. Pantelides, *Phys. Rev. Lett.*, 2007, **99**, 125503.
- 17 J. P. Schaffer, A. J. Perry and J. Brunner, *J. Vac. Sci. Technol., A*, 1992, **10**, 193.
- 18 P. E. Schmid, M. S. Sunaga and F. Lévy, *J. Vac. Sci. Technol., A*, 1998, **16**, 2870.
- 19 Z. Dridi, B. Bouhafs, P. Ruterana and H. Aourag, *J. Phys.: Condens. Matter*, 2002, **14**, 10237.
- 20 M. Tsujimoto, H. Kurata, T. Nemoto, S. Isoda, S. Terada and K. Kaji, *J. Electron Spectrosc. Relat. Phenom.*, 2005, **143**, 159.
- 21 M. Guemmaz, A. Mosser and J.-C. Parlebas, *J. Electron Spectrosc. Relat. Phenom.*, 2000, **107**, 91.
- 22 A. Barnard, *J. Comput. Theor. Nanosci.*, 2004, **1**, 334.
- 23 L. M. Liu, S. Q. Wang and H. Q. Ye, *Acta Mater.*, 2004, **52**, 3681.
- 24 D. Gall, S. Kodambaka, M. A. Wall, I. Petrov and J. E. Greene, *J. Appl. Phys.*, 2003, **93**, 9086.
- 25 C. Wang, Y. Dai, H. Gao, X. Ruan, J. Wang and B. Sun, *Solid State Commun.*, 2010, **150**, 1370.
- 26 A. Soon, M. Todorova, B. Delley and C. Stampfl, *Phys. Rev. B: Condens. Matter Mater. Phys.*, 2007, **75**, 125420.
- 27 M. Fronzi, A. Soon, B. Delley, E. Traversa and C. Stampfl, *J. Chem. Phys.*, 2009, **131**, 104701.
- 28 B. Delley, *J. Chem. Phys.*, 1990, **92**, 508.
- 29 B. Delley, *J. Chem. Phys.*, 2000, **113**, 7756.
- 30 J. P. Perdew, K. Burke and M. Ernzerhof, *Phys. Rev. Lett.*, 1996, **77**, 3865.
- 31 R.-Q. Zhang, C.-E. Kim, B. Delley, C. Stampfl and A. Soon, *Phys. Chem. Chem. Phys.*, 2012, **14**, 2462.
- 32 K. Reuter, C. Stampfl and M. Scheffler, *Ab initio Atomistic Thermodynamics and Statistical Mechanics of Surface Properties and Functions*, in *Handbook of Materials Modeling, Volume 1, Fundamental Models and Methods*, Springer Berlin Heidelberg, 2005.
- 33 C. Stampfl, *Catal. Today*, 2005, **105**, 17.
- 34 A. Soon, M. Todorova, B. Delley and C. Stampfl, *Phys. Rev. B: Condens. Matter Mater. Phys.*, 2006, **73**, 165424.
- 35 K.-P. Bohnen, R. Heid, L. Pintschovius, A. Soon and C. Stampfl, *Phys. Rev. B: Condens. Matter Mater. Phys.*, 2009, **80**, 134304.
- 36 G. Wulff, *Z. Kristallogr.*, 1901, **34**, 449.
- 37 C. Herring, *Phys. Rev.*, 1951, **82**, 87.
- 38 C. L. Cleveland and U. Landman, *J. Chem. Phys.*, 1991, **94**, 7376.
- 39 C. Stampfl, W. Mannstadt, R. Asahi and A. J. Freeman, *Phys. Rev. B: Condens. Matter Mater. Phys.*, 2001, **63**, 155106.
- 40 V. A. Gubanov and A. L. Ivanovsky, *Electronic Structure of Refractory Carbides and Nitrides*, Cambridge University Press, 1994.
- 41 A. Soon, L. Wong, B. Delley and C. Stampfl, *Phys. Rev. B: Condens. Matter Mater. Phys.*, 2008, **77**, 125423.
- 42 M. D. Bentzon and F. Kragh, *Z. Phys. D: At., Mol. Clusters*, 1991, **19**, 299.

Cite this: *Phys. Chem. Chem. Phys.*, 2012, **14**, 16552–16557

www.rsc.org/pccp

PAPER

The role of titanium nitride supports for single-atom platinum-based catalysts in fuel cell technology†

Ren-Qin Zhang,^a Tae-Hun Lee,^a Byung-Deok Yu,^b Catherine Stampfl^c and Aloysius Soon^{*a}

Received 17th April 2012, Accepted 14th June 2012

DOI: 10.1039/c2cp41392b

As a first step towards a microscopic understanding of single-Pt atom-dispersed catalysts on non-conventional TiN supports, we present density-functional theory (DFT) calculations to investigate the adsorption properties of Pt atoms on the pristine TiN(100) surface, as well as the dominant influence of surface defects on the thermodynamic stability of platinized TiN. Optimized atomic geometries, energetics, and analysis of the electronic structure of the Pt/TiN system are reported for various surface coverages of Pt. We find that atomic Pt does not bind preferably to the clean TiN surface, but under typical PEM fuel cell operating conditions, *i.e.* strongly oxidizing conditions, TiN surface vacancies play a crucial role in anchoring the Pt atom for its catalytic function. Whilst considering the energetic stability of the Pt/TiN structures under varying N conditions, embedding Pt at the surface N-vacancy site is found to be the most favorable under N-lean conditions. Thus, the system of embedding Pt at the surface N-vacancy sites on TiN(100) surfaces could be promising catalysts for PEM fuel cells.

Introduction

Heterogeneous catalysis has received a tremendous amount of interest, both from a scientific and industrial perspective. Due to the enormous scale of commercial applications, progress in catalysis can have a positive economic as well as environmental impact, particularly in the area of clean energy technologies. More specifically, the automotive and power generation (*e.g.* fuel cells) industries are the sectors that stand to benefit most directly from breakthroughs that are expected to occur in the field of catalysis. Amongst the various types of fuel cells studied thus far, proton exchange membrane fuel cells (PEMFCs) have received broad attention due to their low operating temperature, low weight, low emissions and quick start-up time.^{1,2} However, there still exist some challenges that hinder their large-scale commercialization, such as the use of the expensive platinum (Pt) catalyst, carbon monoxide (CO) poisoning of this Pt catalyst, as well as severe carbon electrode corrosion.³ In essence, two major drawbacks for the efficient use of PEMFC are namely, its high production costs (due to the use of the Pt catalyst) and its low material durability (resulting in poor lifecycling).⁴ In order to increase the efficiency on a per Pt atom

basis in Pt-based heterogeneous catalysts, one may attempt to increase the surface-to-volume ratio of Pt-based nanocatalysts – confining Pt to the surface as surface-active atoms. There have been various approaches concerning the reduction of Pt *via* nanostructuring, such as decreasing the size of Pt nanoparticles,^{1,4} using a monolayer of Pt in core-shell nanoparticles,^{5,6} or replacing it with non-Pt metals for electrode fabrication.^{3,7}

Another aspect that greatly influences the performance of an electrocatalyst is the nature of the support material. Given the harsh corrosive operational conditions of the PEMFC, the search is on for high-performance, durable materials that are required to withstand the degradation caused due to acidic and oxidizing conditions. The ideal catalyst support material should thus be corrosion-resistant under strongly oxidizing conditions of the PEMFC. Known for its good electrical conductivity and its high resistance to corrosion and acid-attack,⁸ titanium nitride (TiN, see Fig. 1a) is thus considered one of the best candidates for the metallic support material in PEMFCs,⁹ and methanol direct fuel cells,¹⁰ demonstrating clear advantages over traditionally used carbon-based supports which are prone to electrode degradation in a strong acidic medium.¹ In particular, nanoparticles of TiN have been used as a catalyst support material for PEMFCs and they demonstrate higher catalytic performance than conventional platinized carbon electrocatalysts.¹¹ Also, TiN has been proposed as a substrate for electrodeposition of metals such as Pt and Pd.^{12–14} However, detailed surface mechanisms (at the atomic-scale) are still clearly lacking which are crucial for durable materials development.

^a Department of Materials Science & Engineering, Yonsei University, Seoul 120-749, Korea. E-mail: aloysius.soon@yonsei.ac.kr

^b Department of Physics, University of Seoul, Seoul 130-743, Korea

^c School of Physics, The University of Sydney, Sydney NSW 2006, Australia

† This article was submitted as part of a collection on Computational Catalysis and Materials for Energy Production, Storage and Utilization.

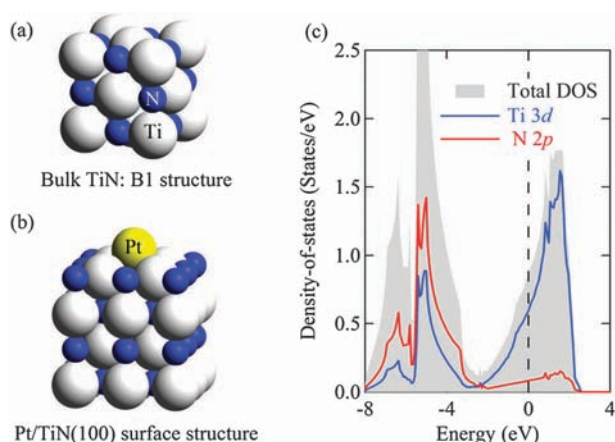


Fig. 1 The crystal structure of bulk titanium nitride, TiN, and the atomic structure model of Pt embedded in an N vacancy site on the TiN(100) surface are shown in (a) and (b), respectively. The platinum, titanium and nitrogen atoms are shown as large yellow, large white and small blue spheres, respectively. (c) The calculated partial density-of-states (PDOSs) of bulk TiN. The Fermi energy is indicated by the vertical dashed line at 0 eV.

In view of all the above-mentioned requirements, we hereby propose one possible design strategy, *i.e.* to combine the use of a durable support material such as TiN and to employ the concept of “single-atom” catalysis which will attempt to reduce the loading of the Pt catalyst in PEMFCs, as well as increasing its per-atom efficiency.

The concept of “single-atom catalysis” was first coined by Sir John Meurig Thomas.¹⁵ The single-atom catalyst not only has an extremely high atom efficiency and activity,¹⁶ but is also a promising way to reduce the high cost of commercial noble-metal catalysts in industry. Recently, Qiao *et al.* have demonstrated experimentally that single Pt atoms could be uniformly dispersed on an FeO_x support of high surface area.¹⁷ The stabilization of single Pt atoms is believed to be due to the electron transfer from Pt atoms to the FeO_x surface. This charge-transfer mechanism could well be extended to other substrates,^{19,20} *e.g.* a nitride support which is studied in this work.^{18,19} Electrodeposition of Pt metal on TiN substrates²⁰ also shows good electrical conductivity of, and connectivity between, the deposited Pt and the TiN substrate. Thus, single Pt atoms dispersed on the TiN substrate is expected to be a promising electrode system for PEMFCs.²¹ However, again, an atomic-level understanding of the Pt/TiN system is still unknown, such as the explicit chemistry for on-surface anchoring or in-surface embedding of Pt atoms on the TiN support.

It is evident that first-principles density-functional theory (DFT) calculations have a distinct advantage of investigating the energetics of atomic-level processes (*e.g.* in heterogeneous catalysis) with high-level precision, as well as providing quantum mechanical-based insights to the associated electronic structure of these processes, *e.g.* how electron transfer could affect the reactivities of Pt/substrate catalysts.^{18,23} Thus, in this work, we use first-principles DFT calculations to understand the fundamental properties of the Pt/TiN electrode system to aid in the rational design of the next generation of PEMFCs. Optimized atomic geometries, energetics, and analysis of the electronic structure of the Pt/TiN system are reported for various surface

coverages of Pt. We find that atomic Pt does not bind preferably to the clean TiN(100) surface, but under typical PEM fuel cells operational conditions, *i.e.* strongly oxidizing conditions,^{3,4} TiN surface vacancies (*e.g.* V_N) play a crucial role in anchoring the Pt atom for its catalytic function.

Computational method

For all DFT calculations, we use the Vienna *Ab initio* Simulations Package (VASP 5.2) code.^{22,23} We employ the projector augmented-wave (PAW) method²⁴ for the electron–ion interactions and the generalized-gradient approximation (GGA) due to Perdew, Burke and Ernzerhof (PBE)²⁵ for the exchange–correlation functional. With its PAW potentials, VASP combines the accuracy of all-electron methods with the computational efficiency of plane-wave approaches. The electronic wave functions are expanded in a basis set of plane waves with a kinetic-energy cutoff of 500 eV. In order to study the effect of the adsorption of Pt atoms on the electronic structure and properties of the TiN(100) surface as a function of surface coverage Θ , we use a periodic slab model consisting of four atomic layers with a vacuum region of about 12 Å (See Fig. 1b). We find that upon increasing the number of atomic layers to six layers, the difference in binding energy is found to be less than 0.02 eV/Pt atom. The different surface coverages are modeled using $p(1 \times 1)$, $p(2 \times 2)$, $p(3 \times 3)$, $p(4 \times 4)$ surface cells, where we consider $\Theta = 0.06$ to 1.00 ML. We define Θ as the ratio of the number of Pt atoms to the number of TiN units in the unit cell of an ideal TiN surface. Pt atoms and the top two atomic layers are allowed to fully relax while keeping the bottom two layers fixed. We consider adsorption in various on-surface sites and surface vacancy sites (substitutional adsorption). The \mathbf{k} -space integration is performed using $12 \times 12 \times 1$, $6 \times 6 \times 1$, $4 \times 4 \times 1$, $3 \times 3 \times 1$ meshes in the Brillouin zone for the $p(1 \times 1)$, $p(2 \times 2)$, $p(3 \times 3)$, $p(4 \times 4)$ surface cells, respectively. A Methfessel-Paxton smearing of 0.1 eV is used to improve the convergence and the total energy is extrapolated back to zero temperature. Dipole corrections²⁶ to the electrostatic potential and total energy are imposed to eliminate dipole–dipole interactions of images between supercells. The convergence criterion for the total energy is taken to be smaller than 1×10^{-5} eV, while for geometry optimization, the ionic relaxations are performed until the net change in the forces acting on the atoms becomes smaller than 1×10^{-2} eV Å⁻¹.

In order to investigate the thermodynamic stability of Pt adsorption in on-surface sites and surface vacancy sites, we define the average binding energy per Pt atom, E_{Pt}^{b} . To address the possibility of bulk-like clustering behavior of Pt on TiN(100), E_{Pt}^{b} is calculated with respect to the total energy of bulk Pt $E_{\text{Pt}}^{\text{bulk}}$. The chemical potentials of N under different chemical environments can strongly affect the properties of Pt/TiN surfaces. Given that the operating conditions of PEMFCs are typically under strongly oxidizing conditions,^{3,4} in this work we will address the stability of the Pt/TiN(100) structures under low chemical potential of N, μ_N conditions as a first approximation to these harsh oxidizing conditions. To estimate the thermodynamic stability of single Pt atoms adsorbed on clean and defective surfaces of TiN(100), the binding energy of Pt, E_{Pt}^{b} , is calculated,

including the cost of vacancy formation energy, as a function of the chemical potential of N, μ_N . It is defined as

$$E_{\text{Pt}}^{\text{b}} = E_{\text{tot}} - E_{\text{TiN}}^{\text{clean}} - (n\mu_{\text{Ti}} + m\mu_{\text{N}} + l\mu_{\text{Pt}}) \quad (1)$$

where E_{tot} and $E_{\text{TiN}}^{\text{clean}}$ are the total energy of the system for Pt adsorbed on a vacancy site and pure TiN (surface or bulk), respectively; n , m and l are the number of the Ti vacancies, N vacancies and adsorbed Pt atoms, respectively. μ_{Ti} , μ_{N} and μ_{Pt} are the atomic chemical potentials of the Ti, N and Pt, respectively. Here we assume μ_{Pt} as the binding energy of bulk Pt $E_{\text{Pt}}^{\text{bulk}}$. The lower boundary (*i.e.* under N-lean conditions), is taken as the chemical potential of N whereby the spontaneous decomposition of the nitride into titanium metal and nitrogen gas will become favorable, whereas that of the upper boundary (*i.e.* under N-rich conditions) is defined when N_2 condensation takes place on the surface at low temperatures. Thus, under N-lean conditions, $\mu_{\text{Ti}} = E_{\text{Ti}}^{\text{bulk}}$ and $\mu_{\text{N}} = E_{\text{TiN}}^{\text{bulk}} - E_{\text{Ti}}^{\text{bulk}}$, while under N-rich conditions, $\mu_{\text{N}} = \frac{1}{2}E_{\text{N}_2}^{\text{mlc}}$ and $\mu_{\text{Ti}} = E_{\text{TiN}}^{\text{bulk}} - \frac{1}{2}E_{\text{N}_2}$, where $E_{\text{TiN}}^{\text{bulk}}$, $E_{\text{Ti}}^{\text{bulk}}$ and $E_{\text{N}_2}^{\text{mlc}}$ are the total energies of bulk TiN, bulk Ti and the N_2 molecule, respectively. We note that for the stability of a single Pt adsorption in on-surface sites (*i.e.* without vacancy), the binding energy can be calculated by eqn (1) when $n = 0$ and $m = 0$, with $\mu_{\text{Pt}} = E_{\text{Pt}}^{\text{bulk}}$ consistently referred to that of bulk Pt. In eqn (1), a positive binding energy indicates that the adsorption is endothermic, while a negative binding energy indicates that the adsorption is exothermic and thermodynamically more stable than that in bulk Pt.

Results and discussion

Firstly, we calculate the properties of bulk TiN, yielding a lattice constant of 4.249 Å and bulk modulus of 280 GPa, which is consistent with the experimental results of 4.238 Å²⁷ and 288 GPa,²⁸ respectively, as well as the theoretical values of 4.210 Å and 275.5 GPa in our previous work.²⁹ The electronic density-of-states, decomposed into Ti 3d and N 2p states, are shown in Fig. 1c, which shows that TiN is a metal with 0.87 states eV⁻¹ at the Fermi level.⁸ The largely dispersive unoccupied bands are composed of Ti 3d states, while the occupied bands show a strong hybridization of N 2p–Ti 3d states.

The calculated binding energies with respect to the energy of bulk Pt (per Pt atom) vary as function of the surface coverage Θ , which is presented in Fig. 2. For on-surface adsorption at each of the surface coverages, Pt atoms are placed in the top sites (T_{Ti} and T_{N}) and bridge sites (B_{AA} and B_{AB}), as shown in the insert of Fig. 2. It is found that as Θ increases from 0.06 to 0.25 ML, the binding energy at all adsorption sites increases, while for increasing Θ to 1.0 ML, the binding energy decreases. This dramatic variation is attributed to the competition between the Pt-surface and lateral Pt–Pt interactions. When compared to the cohesive energy of bulk Pt, the positive binding energies of Pt at the considered on-surface sites suggest that the cohesive energy of Pt atoms on TiN(100) is less favorable than that in bulk Pt. This suggests that single Pt atom adsorption at these sites is thermodynamically unstable, and driving the atoms to form more favorable bulk-like Pt clusters. Here, we also find adsorbed Pt atoms on TiN(100) are displaced vertically away from the surface by 2.14, 2.28, 2.02,

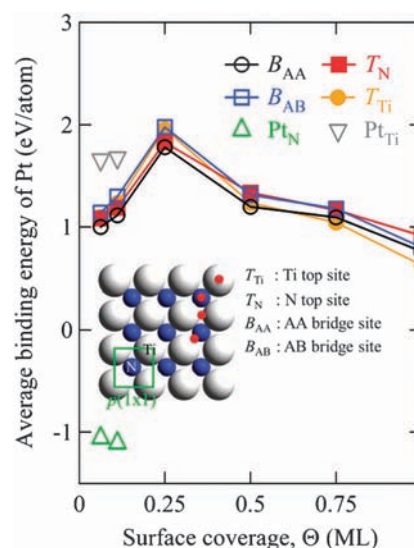


Fig. 2 Calculated binding energies of Pt on TiN(100) surface (calculated by eqn (1)) in the on-surface sites for various coverages. B_{AA} , B_{AB} , T_{N} and T_{Ti} denote the on-surface adsorption sites of AA bridge (*i.e.* a bridge site between two like atoms), AB bridge (*i.e.* a bridge site between an N atom and a Ti atom), N top and Ti top, respectively (as shown in the insert), while Pt_{N} and Pt_{Ti} denote the substitutional adsorption sites of N and Ti vacancies, correspondingly. For the substitutional adsorption, the binding energies calculated by eqn (1) under N-lean conditions for Pt_{N} and N-rich conditions for Pt_{Ti} are shown. For the cases under N-rich conditions for Pt_{N} and N-lean conditions for Pt_{Ti} , the binding energies are large and positive values (see Table 2).

and 2.22 Å for the B_{AA} , B_{AB} , T_{N} , and T_{Ti} sites, respectively (*e.g.* at the 0.06 ML coverage).

However, we note that previous theoretical calculations have reported that nitrogen point defects could influence the stability and induce atomic-scale structural changes in transition-metal nitrides.³⁰ Furthermore, recent studies of iron oxide supported single Pt atoms show that surface vacancies of the supports could well serve as anchoring sites for single Pt atoms.¹⁷ In this work, we study the N (V_{N}) and Ti (V_{Ti}) atom vacancy formation energies of TiN(100) surface and bulk TiN under different nitrogen environments (N-lean and N-rich), which are listed in Table 1. The vacancy formation energy is calculated by eqn (1) when $l = 0$. We find that N vacancies form readily and are exothermic both on the surface and in the bulk under N-lean conditions. Under such conditions, Ti vacancy formation at both the surface and in the bulk is found to be largely endothermic and has a considerable formation

Table 1 The N (V_{N}) and Ti (V_{Ti}) vacancy formation energy for vacancies at the TiN(100) surface and in bulk TiN, under different conditions (N-lean and N-rich). $p(3 \times 3)$ and $p(4 \times 4)$ are the size of the surface unit cell, which represents different vacancy surface coverages of 0.11 and 0.06 ML, respectively. For bulk TiN, a $(3 \times 3 \times 3)$ supercell is used, which is found to be sufficiently large to exclude the interaction between vacancies (we have checked with a bulk $(4 \times 4 \times 4)$ supercell and the conclusion was not changed)

V_{N} (eV)	N-lean	N-rich	V_{Ti} (eV)	N-lean	N-rich
$p(3 \times 3)$	−0.42	3.02	$p(3 \times 3)$	3.40	−0.04
$p(4 \times 4)$	−0.37	3.07	$p(4 \times 4)$	3.45	0.00
Bulk $(3 \times 3 \times 3)$	−0.87	2.58	Bulk $(3 \times 3 \times 3)$	2.96	−0.49

energy of $\sim 3\text{--}3.5$ eV. On the other hand, under N-rich conditions, N vacancies are difficult to form, yielding a large formation energy of $\sim 2.5\text{--}3$ eV. The formation of Ti vacancies, however, is found to be slightly easier than that of N vacancies, but their formation energy is marginally exothermic. We have also found that a nitrogen mono-vacancy is considerably easier to form on TiN(100) than a di-vacancy, under N-lean conditions.³¹

The high stability of surface vacancies under certain conditions has prompted us to further investigate the adsorption properties of Pt at these sites. We considered so-called substitutional adsorption of Pt atoms in the Ti and N vacancy sites, which are labeled Pt_{Ti} and Pt_{N} , respectively. Again, as shown in Fig. 2, the binding energies at all other considered sites are always positive with respect to that of bulk Pt, with the exception of Pt adsorption at the N vacancy site (Pt_{N}) under N-lean conditions. This leads us to believe that the binding of Pt to TiN surfaces is strongly mediated *via* these surface V_{N} , highlighting the importance of surface defects for this system. When compared to the cohesive energy of bulk Pt, the negative binding energy of Pt at V_{N} implies that the cohesive energy of a Pt atom on defective TiN(100) is higher than that of bulk Pt atoms. Nevertheless, the positive binding energy of Pt adsorption at V_{Ti} under N-rich conditions denotes that the Ti vacancy site is unfavorable for Pt adsorption, even when compared to on-surface Pt adsorption. Concerning the atomic structures, for the Pt_{N} system, the vertical displacement of Pt from the TiN(100) surface is found to be 1.41 \AA (and bond length of Pt–Ti, $d_{\text{Pt-Ti}}$ is 2.66 \AA), while that of the Pt_{Ti} system is found to be 0.30 \AA (and $d_{\text{Pt-N}}$ is 2.17 \AA).

In a nutshell, Pt atoms prefer to be “embedded” on the surface of TiN(100) only at the V_{N} site, while all other on-surface adsorptions are largely unfavourable with respect to bulk Pt. This somewhat resembles the result of Pt single atoms bound to the Fe_2O_3 surface, as seen in experiments.¹⁷

Given that the diffusion of Pt into the carbon supports is one of the well-known reasons for poor efficiencies of Pt/carbon catalysts, we find it necessary to check the thermodynamic stability of Pt atoms in bulk TiN. To check this, we calculate the binding energy of Pt_{Ti} and Pt_{N} in bulk TiN using a $(3 \times 3 \times 3)$ bulk TiN supercell, *i.e.* substituting a Pt atom at the Ti, and N site, respectively. In Table 2, we list the atomic binding energy of Pt atoms adsorbed on the N and Ti surface vacancy sites under N-lean and N-rich conditions, compared to that in bulk TiN. For Pt in both the N and Ti vacancy sites of bulk TiN, the positive and large binding energies indicate that it is thermodynamically very unlikely for Pt atoms to occupy N and Ti sites of bulk TiN. These large positive

values are attributed to the large size mismatch between Pt and the smaller N and Ti atoms in bulk TiN. In addition, the binding energies of Pt_{N} at the TiN surface are very similar for both the $p(3 \times 3)$ and $p(4 \times 4)$ surface unit cells, *i.e.* for coverages of 0.11 and 0.06 ML, respectively. This indicates that the $p(3 \times 3)$ surface unit cell should be large enough to minimize the lateral interactions between Pt atoms. Thus, we can conclude that Pt atoms can be stably embedded in the N vacancy site of TiN(100) surface, without forming bulk-like Pt clusters, nor diffusing into bulk TiN. From a thermodynamic point-of-view, the Pt/TiN system could offer a possible route to improve the efficiencies of Pt-based nanocatalysts for the PEMFC.

In Fig. 3, with increasing chemical potential of N, μ_{N} , *i.e.* from N-lean to N-rich conditions, the binding energy of Pt at the N vacancy increases, while that of Pt at the Ti vacancy decreases. It can be seen that when $\Delta\mu_{\text{N}} < -2.33$ eV, Pt_{N} at TiN(100) is the only system for which the binding energy is found to be negative, *i.e.* thermodynamically stable. With increasing μ_{N} , the binding energy of Pt_{N} at TiN(100) increases and finally becomes positive and larger than that of Pt adsorbed on the surface of clean TiN(100) (average on-surface adsorption: $E_{\text{b}} = 1.21$ eV) when $\Delta\mu_{\text{N}} > -1.12$ eV. Thus, it can be inferred that Pt at the surface N-vacancy is the most favorable system under N-lean conditions, and as μ_{N} increases, it becomes increasingly less favorable, and ends up being less stable than the on-surface adsorption systems. Considering the energetic stability of the Pt/TiN structures under varying N conditions, it is concluded that embedding Pt at the surface N-vacancy site is the most favorable under N-lean conditions,

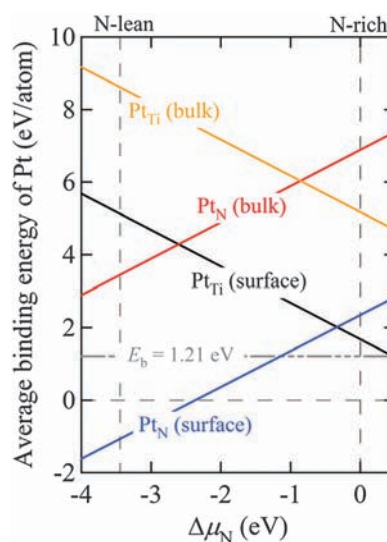


Fig. 3 According to eqn (1), the binding energy of Pt, E_{Pt} , in the bulk and surface N- and Ti-vacancy sites changes as a function of chemical potential of N, μ_{N} , for the $(3 \times 3 \times 3)$ bulk TiN and the $p(3 \times 3)$ TiN(100) systems. $\Delta\mu_{\text{N}}$ is defined by $\Delta\mu_{\text{N}} = \mu_{\text{N}} - \frac{1}{2} E_{\text{N}_2}^{\text{mlc}}$, where $E_{\text{N}_2}^{\text{mlc}}$ is the total energy of the N_2 molecule. The thermodynamically allowed range of $\Delta\mu_{\text{N}}$ is between -3.45 eV (N-lean) and 0.00 eV (N-rich). Pt_{N} and Pt_{Ti} denote the substitutional adsorption sites of N and Ti vacancies in the TiN bulk and surface, respectively. The dot dashed line denotes the average binding energy of Pt for the situation of on-surface adsorption of the $p(3 \times 3)$ TiN(100) system, in the most favorable site, which is 1.21 eV.

Table 2 The binding energy of Pt atoms adsorbed on N and Ti vacancy sites at the TiN(100) surface and in bulk TiN, which are denoted by Pt_{N} and Pt_{Ti} , respectively (calculated by eqn (1)). $p(3 \times 3)$ and $p(4 \times 4)$ are the surface unit cells used, which represent different Pt surface coverages of 0.11 and 0.06 ML, respectively. For bulk TiN, a supercell of $(3 \times 3 \times 3)$ is used, containing 54 atoms, which is large enough to exclude the interaction between Pt atoms

E_{Pt}^{b} (eV)	Pt_{N}		Pt_{Ti}	
	N-lean	N-rich	N-lean	N-rich
$p(3 \times 3)$	−1.11	2.33	5.12	1.68
$p(4 \times 4)$	−1.06	2.38	5.11	1.66
Bulk $(3 \times 3 \times 3)$	3.44	6.89	7.64	4.19

which seems to be a reasonable first approximation to strongly oxidizing conditions (*i.e.* close to PEMFC operating conditions).

To provide further insight into the electronic structure of the systems, we consider the partial density-of-states of Pt atoms adsorbed in both Ti and N vacancy sites, as shown in Fig. 4. In both cases, we observe a renormalization of Pt 5d states, compared with Pt 5d states of the clean Pt(100) surface and bulk Pt. The stability of Pt adsorbed on the N vacancy site is reflected in the lower energy position of the electronic states, which are mainly distributed in the range from -3 to -2 eV, compared to that of Pt adsorbed on the Ti vacancy site, which are mainly distributed in the range from -2 to -1 eV. We also calculated the d band centre, ε_d , of Pt and Ti atoms in the different systems, as shown in Table 3. For Pt_N , the ε_d of Pt 5d bands in the Pt_N system is lower than that of the Pt_Ti system, because of the interaction between Pt 5d states and Ti 3d states. Simultaneously, the ε_d of the Ti 3d bands for the Pt_N adsorption is higher than that of the Ti 3d bands of the clean TiN(100) surface and bulk TiN.

To further aid our understanding, we discuss this difference *via* plots of charge density differences, as shown in Fig. 5 for the Pt atoms adsorbed on N and Ti vacancy sites of the TiN(100) surface systems. The charge density difference, $\Delta\rho$, can be derived by considering: $\Delta\rho = \rho^\text{sys} - \rho^\text{Pt} - \rho^\text{TiN}$, where ρ^sys , ρ^Pt and ρ^TiN are the charge densities of the supercell Pt/TiN slab system, the Pt atom and the slab of TiN(100) surface with N (or Ti) vacancy, respectively. In calculation of the latter two quantities, the atomic positions are fixed as those they have in the Pt/TiN system. From these redistributions, it is found that for Pt_N , there is a bonding between the Pt and Ti atoms. As we can see, the depletion (blue) of electron density on both the Pt and Ti atoms, and a significant (yellow) accumulation between them. There is a “ring” of negative charge about the Pt atom, which is consistent with our calculated Bader charge result ($-0.49|e|$). For Pt atoms adsorbed on an N vacancy site, it suggests that a single Pt atom embedded into the TiN surface experiences a significant increase in the occupation of the 5d states due to coordination by the four neighboring surface Ti atoms, where the electronegativity

Table 3 The d-band centre, ε_d , with respect to the corresponding Fermi level for the different systems. Pt_Ti and Pt_N denote the systems of Pt adsorbed on Ti and N vacancy sites in the TiN(100) surface, respectively

ε_d (eV)	Bulk Pt	Clean Pt(100)	Pt_Ti	Pt_N	Clean TiN(100)	Bulk TiN
Pt	-3.092	-2.118	-2.158	-2.746	—	—
Ti	—	—	—	-3.946	-4.074	-4.606

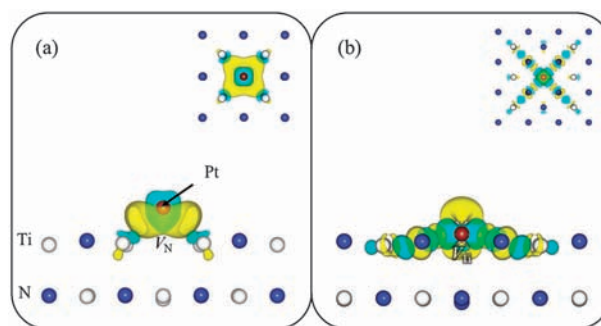


Fig. 5 A side-view of electron charge density differences for the substitutional adsorption of Pt atoms on the (a) N and (b) Ti vacancy sites, respectively, where the inset shows the corresponding top-view. Charge accumulation and depletion are represented by the yellow and light blue regions, respectively. The isosurface levels are set to ± 0.005 e bohr $^{-3}$.

of Pt (Pauling value of 2.28) is larger than that of Ti (Pauling value of 1.54). The charge transfer is localized around Pt and Ti atoms. For Pt atom adsorption on Ti vacancies, the charge redistribution is directional and both N and Ti atoms are involved in the charge transfer. Also, there is some kind of directional interaction between the Pt and N atoms; one of the main effects is considered to be a depletion of the planar Pt 5d states, and increase into the perpendicular d_{zz} states. This could give rise to the (presumably) anti-bonding type Pt states at/near the Fermi level (seen in Fig. 4b), which result in the unfavorable Pt adsorption energy.

As a first step towards the atomic and electronic understanding of single-Pt atom-dispersion on TiN surfaces for catalysts in

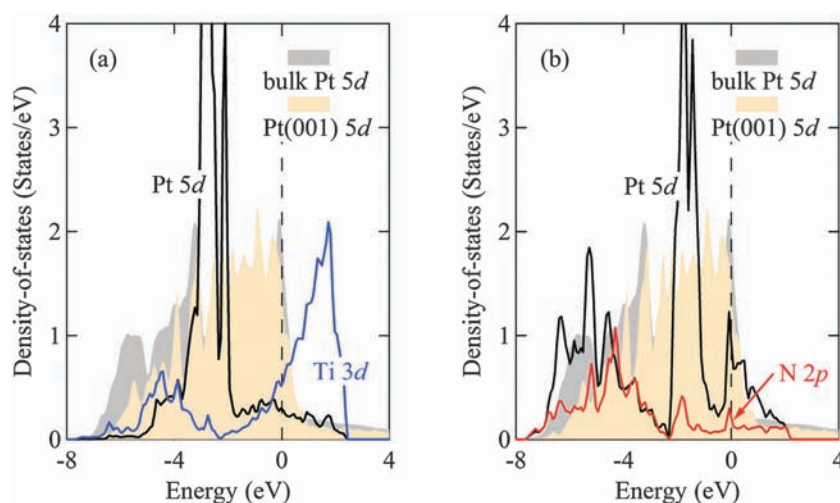


Fig. 4 The partial density-of-states for Pt atoms adsorbed on (a) an N vacancy site, and (b) a Ti vacancy site. The Fermi energy is indicated by the vertical dash line at 0 eV.

PEMFC, by using first-principle calculations, we study the stability of single-Pt atoms on the (100) surface of the non-conventional support material TiN. Single-Pt atoms prefer to occupy the N vacancy sites in the TiN surface under N-lean conditions. In order to realize the application of this platinized TiN surface in PEMFCs, further research is being pursued to investigate the stability of Pt/TiN electrodes in different electrolytes *via* surface Pourbaix diagrams.

Conclusion


In summary, utilizing first-principles DFT calculations, TiN supports for single-atom platinum-based catalysts are investigated. It is found that a Pt atom prefers to be embedded in the surface of TiN at the N vacancy sites. According to the binding energy of Pt atoms, with respect to that of bulk Pt, single Pt atoms could be stable on the N atomic vacancy site rather than forming Pt metal clusters. The substitutional adsorption of Pt atoms at Ti vacancy sites in bulk TiN is energetically unfavorable. We found that atomic Pt does not bind preferably to the clean TiN surface, but under typical PEM fuel cells operational conditions, *i.e.* strongly oxidizing conditions, TiN surface vacancies play a crucial role in anchoring the Pt atom for its catalytic function. Whilst considering the energetic stability of the Pt/TiN structures under varying N conditions, embedding Pt at the surface N-vacancy site is found to be the most favorable under N-lean conditions, where Pt presents negative charge.

Acknowledgements

The authors gratefully acknowledge support through a financial award provided by the Asian Office of Aerospace Research and Development (AOARD, Award No. FA2386-12-1-4017), and the Australian Research Council (ARC). Computational resources have been provided by the Korea Institute of Science and Technology Information (KISTI) supercomputing center through the strategic support program for the supercomputing application research (KSC-2011-C2-39), as well as the Australian National Computational Infrastructure (NCI). RQZ acknowledges the Second Stage of Brain Korea 21 Project (Division of Human-electronics Information Materials) for funding.

References

- 1 D. Ham and J. Lee, *Energies*, 2009, **2**, 873–899.
- 2 D. Anne-Claire, *Prog. Mater. Sci.*, 2011, **56**, 289–327.
- 3 R. Bashyam and P. Zelenay, *Nature*, 2006, **443**, 63–66.
- 4 H. A. Gasteiger, S. S. Kocha, B. Sompalli and F. T. Wagner, *Appl. Catal., B*, 2005, **56**, 9–35.
- 5 M. H. Huang, G. F. Dong, N. Wang, J. X. Xu and L. H. Guan, *Energy Environ. Sci.*, 2011, **4**, 4513–4516.
- 6 K. A. Kuttiyil, K. Sasaki, Y. Choi, D. Su, P. Liu and R. R. Adzic, *Energy Environ. Sci.*, 2012, **5**, 5297–5304.
- 7 Y. Liang, Y. Li, H. Wang, J. Zhou, J. Wang, T. Regier and H. Dai, *Nat. Mater.*, 2011, **10**, 780–786.
- 8 C. Stampfl, W. Mannstadt, R. Asahi and A. J. Freeman, *Phys. Rev. B: Condens. Matter*, 2001, **63**, 155106.
- 9 B. Avasarala and P. Haldar, *Electrochim. Acta*, 2010, **55**, 9024–9034.
- 10 M. M. Ottakam Thotiyl, T. Ravikumar and S. Sampath, *J. Mater. Chem.*, 2010, **20**, 10643–10651.
- 11 B. Avasarala, T. Murray, W. Li and P. Haldar, *J. Mater. Chem.*, 2009, **19**, 1803–1805.
- 12 O. T. M. Musthafa and S. Sampath, *Chem. Commun.*, 2008, 67–69.
- 13 M. M. O. Thotiyl, T. R. Kumar and S. Sampath, *J. Phys. Chem. C*, 2010, **114**, 17934–17941.
- 14 M. M. O. Thotiyl and S. Sampath, *Electrochim. Acta*, 2011, **56**, 3549–3554.
- 15 J. M. Thomas, R. Raja and D. W. Lewis, *Angew. Chem., Int. Ed.*, 2005, **44**, 6456–6482.
- 16 Y. Zhai, D. Pierre, R. Si, W. Deng, P. Ferrin, A. U. Nilekar, G. Peng, J. A. Herron, D. C. Bell, H. Saltsburg, M. Mavrikakis and M. Flytzani-Stephanopoulos, *Science*, 2010, **329**, 1633–1636.
- 17 B. Qiao, A. Wang, X. Yang, L. F. Allard, Z. Jiang, Y. Cui, J. Liu, J. Li and T. Zhang, *Nat. Chem.*, 2011, **3**, 634–641.
- 18 J. M. Thomas, Z. Saghi and P. L. Gai, *Top. Catal.*, 2011, **54**, 588–594.
- 19 J. H. Kwak, J. Hu, D. Mei, C.-W. Yi, D. H. Kim, C. H. F. Peden, L. F. Allard and J. Szanyi, *Science*, 2009, **325**, 1670–1673.
- 20 S. A. G. Evans, J. G. Terry, N. O. V. Plank, A. J. Walton, L. M. Keane, C. J. Campbell, P. Ghazal, J. S. Beattie, T.-J. Su, J. Crain and A. R. Mount, *Electrochem. Commun.*, 2005, **7**, 125–129.
- 21 J. M. Thomas, *Angew. Chem., Int. Ed.*, 2011, **50**, 49–50.
- 22 G. Kresse and J. Hafner, *Phys. Rev. B: Condens. Matter*, 1993, **47**, 558.
- 23 G. Kresse and J. Furthmüller, *Phys. Rev. B: Condens. Matter*, 1996, **54**, 11169.
- 24 G. Kresse and D. Joubert, *Phys. Rev. B: Condens. Matter Mater. Phys.*, 1999, **59**, 1758–1775.
- 25 J. P. Perdew, K. Burke and M. Ernzerhof, *Phys. Rev. Lett.*, 1996, **77**, 3865.
- 26 G. Makov and M. C. Payne, *Phys. Rev. B: Condens. Matter*, 1995, **51**, 4014.
- 27 N. Schönberg, *Acta Chem. Scand.*, 1954, **08**, 213–220.
- 28 M. Marlo and V. Milman, *Phys. Rev. B: Condens. Matter*, 2000, **62**, 2899.
- 29 R. Q. Zhang, C.-E. Kim, B. Delley, C. Stampfl and A. Soon, *Phys. Chem. Chem. Phys.*, 2012, **14**, 2462–2467.
- 30 L. Tsetseris, N. Kalfagiannis, S. Logothetidis and S. T. Pantelides, *Phys. Rev. Lett.*, 2007, **99**, 125503.
- 31 T.-H. Lee, B. Delley, C. Stampfl and A. Soon, *Nanoscale*, DOI: 10.1039/C2NR31266B.

REPORT OF INVENTIONS AND SUBCONTRACTS <i>(Pursuant to "Patent Rights" Contract Clause) (See Instructions on back)</i>							Form Approved OMB No. 9000-0095 Expires Jan 31, 2008		
The public reporting burden for this collection of information is estimated to average 1 hour per response, including the time for reviewing instructions, searching existing data sources, gathering and maintaining the data needed, and completing and reviewing the collection of information. Send comments regarding this burden estimate or any other aspect of this collection of information, including suggestions for reducing the burden, to the Department of Defense, Executive Services Directorate (9000-0095). Respondents should be aware that notwithstanding any other provision of law, no person shall be subject to any penalty for failing to comply with a collection of information if it does not display a currently valid OMB control number.									
PLEASE DO NOT RETURN YOUR COMPLETED FORM TO THE ABOVE ORGANIZATION. RETURN COMPLETED FORM TO THE CONTRACTING OFFICER.									
1.a. NAME OF CONTRACTOR/SUBCONTRACTOR YONSEI UNIVERSITY Industry Academic		c. CONTRACT NUMBER FA2386-12-1-4107		2.a. NAME OF GOVERNMENT PRIME CONTRACTOR		c. CONTRACT NUMBER		3. TYPE OF REPORT (X one) a. INTERIM <input checked="" type="checkbox"/> b. FINAL <input type="checkbox"/>	
b. ADDRESS (Include ZIP Code) Cooperation Foundation 50, Yonsei-Ro, Seodaemun-Gu, SEOUL, 120-749, KOREA		d. AWARD DATE (YYYYMMDD) 20120130		b. ADDRESS (Include ZIP Code)		d. AWARD DATE (YYYYMMDD)		4. REPORTING PERIOD (YYYYMMDD) a. FROM 20120130 b. TO 20130129	
SECTION I - SUBJECT INVENTIONS									
5. "SUBJECT INVENTIONS" REQUIRED TO BE REPORTED BY CONTRACTOR/SUBCONTRACTOR (If "None," so state)									
NAME(S) OF INVENTOR(S) <i>(Last, First, Middle Initial)</i> a.		TITLE OF INVENTION(S) b.		DISCLOSURE NUMBER, PATENT APPLICATION SERIAL NUMBER OR PATENT NUMBER c.		ELECTION TO FILE PATENT APPLICATIONS (X)		CONFIRMATORY INSTRUMENT OR ASSIGNMENT FORWARDED TO CONTRACTING OFFICER (X) e.	
						d.			
						(1) UNITED STATES (a) YES (b) NO		(2) FOREIGN (a) YES (b) NO	
N/A		N/A		N/A				X	
f. EMPLOYER OF INVENTOR(S) NOT EMPLOYED BY CONTRACTOR/SUBCONTRACTOR				g. ELECTED FOREIGN COUNTRIES IN WHICH A PATENT APPLICATION WILL BE FILED					
(1) (a) NAME OF INVENTOR (Last, First, Middle Initial) N/A		(2) (a) NAME OF INVENTOR (Last, First, Middle Initial) N/A		(1) TITLE OF INVENTION N/A		(2) FOREIGN COUNTRIES OF PATENT APPLICATION N/A			
(b) NAME OF EMPLOYER N/A		(b) NAME OF EMPLOYER N/A							
(c) ADDRESS OF EMPLOYER (Include ZIP Code) N/A		(c) ADDRESS OF EMPLOYER (Include ZIP Code) N/A							
SECTION II - SUBCONTRACTS (Containing a "Patent Rights" clause)									
6. SUBCONTRACTS AWARDED BY CONTRACTOR/SUBCONTRACTOR (If "None," so state)									
NAME OF SUBCONTRACTOR(S) a.		ADDRESS (Include ZIP Code) b.		FAR "PATENT RIGHTS" d.		DESCRIPTION OF WORK TO BE PERFORMED UNDER SUBCONTRACT(S) e.		SUBCONTRACT DATES (YYYYMMDD) f.	
				(1) CLAUSE NUMBER (2) DATE (YYYYMM)				(1) AWARD (2) ESTIMATED COMPLETION	
N/A		N/A		N/A		N/A			
SECTION III - CERTIFICATION									
7. CERTIFICATION OF REPORT BY CONTRACTOR/SUBCONTRACTOR (Not required if: (X as appropriate))									
				SMALL BUSINESS or		<input checked="" type="checkbox"/> NONPROFIT ORGANIZATION			
I certify that the reporting party has procedures for prompt identification and timely disclosure of "Subject Inventions," that such procedures have been followed and that all "Subject Inventions" have been reported.									
a. NAME OF AUTHORIZED CONTRACTOR/SUBCONTRACTOR OFFICIAL (Last, First, Middle Initial) Taesun Park		b. TITLE President of IACF, Yonsei University			c. SIGNATURE 		d. DATE SIGNED 20130205		

FEDERAL FINANCIAL REPORT

(Follow form instructions)

1. Federal Agency and Organizational Element to Which Report is Submitted ASIAN OFFICE OF AEROSPACE R&D (AOARD)	2. Federal Grant or Other Identifying Number Assigned by Federal Agency (To report multiple grants, use FFR Attachment) FA2386-12-1-4017	Page 1 of 1 pages
---	---	---------------------------------

3. Recipient Organization (Name and complete address including Zip code) YONSEI UNIVERSITY Industry Academic Cooperation Foundation 50, Yonsei-Ro, Seodaemun-Gu, SEOUL, 120-749, KOREA

4a. DUNS Number 631085094	4b. EIN N/A	5. Recipient Account Number or Identifying Number (To report multiple grants, use FFR Attachment) N/A	6. Report Type <input type="checkbox"/> Quarterly <input type="checkbox"/> Semi-Annual <input type="checkbox"/> Annual <input checked="" type="checkbox"/> Final	7. Basis of Accounting <input checked="" type="checkbox"/> Cash <input type="checkbox"/> Accrual
-------------------------------------	-----------------------	--	---	--

8. Project/Grant Period From: (Month, Day, Year) 01302012	To: (Month, Day, Year) 01292013	9. Reporting Period End Date (Month, Day, Year) 01292013
--	------------------------------------	---

10. Transactions	Cumulative
-------------------------	------------

(Use lines a-c for single or multiple grant reporting)

Federal Cash (To report multiple grants, also use FFR Attachment):	
a. Cash Receipts	50,000
b. Cash Disbursements	50,000
c. Cash on Hand (line a minus b)	0

(Use lines d-o for single grant reporting)

Federal Expenditures and Unobligated Balance:	
d. Total Federal funds authorized	50,000
e. Federal share of expenditures	50,000
f. Federal share of unliquidated obligations	0
g. Total Federal share (sum of lines e and f)	50,000
h. Unobligated balance of Federal funds (line d minus g)	0

Recipient Share:	
i. Total recipient share required	0
j. Recipient share of expenditures	0
k. Remaining recipient share to be provided (line i minus j)	0

Program Income:	
l. Total Federal program income earned	0
m. Program income expended in accordance with the deduction alternative	0
n. Program income expended in accordance with the addition alternative	0
o. Unexpended program income (line l minus line m or line n)	0

11. Indirect Expense	a. Type	b. Rate	c. Period From	Period To	d. Base	e. Amount Charged	f. Federal Share
	N/A	N/A	N/A	N/A	N/A	N/A	N/A
	g. Totals:					N/A	N/A

12. Remarks: Attach any explanations deemed necessary or information required by Federal sponsoring agency in compliance with governing legislation: N/A
--

13. Certification: By signing this report, I certify that it is true, complete, and accurate to the best of my knowledge. I am aware that any false, fictitious, or fraudulent information may subject me to criminal, civil, or administrative penalties. (U.S. Code, Title 18, Section 1001)

a. Typed or Printed Name and Title of Authorized Certifying Official Taesun Park / President of IACF, Yonsei University	c. Telephone (Area code, number and extension) +82 2 2123 5186
b. Signature of Authorized Certifying Official 	d. Email address tspark@yonsei.ac.kr
	e. Date Report Submitted (Month, Day, Year) 02052013
14. Agency use only:	

Standard Form 425
 OMB Approval Number: 0348-0061
 Expiration Date: 10/31/2011

Paperwork Burden Statement

According to the Paperwork Reduction Act, as amended, no persons are required to respond to a collection of information unless it displays a valid OMB Control Number. The valid OMB control number for this information collection is 0348-0061. Public reporting burden for this collection of information is estimated to average 1.5 hours per response, including time for reviewing instructions, searching existing data sources, gathering and maintaining the data needed, and completing and reviewing the collection of information. Send comments regarding the burden estimate or any other aspect of this collection of information, including suggestions for reducing this burden, to the Office of Management and Budget, Paperwork Reduction Project (0348-0061), Washington, DC 20503.